CHEST

Clinical Molecular Imaging of Pulmonary CXCR4 Expression to Predict Outcome of Pirfenidone Treatment in Idiopathic Pulmonary Fibrosis

Thorsten Derlin, MD; Benedikt Jaeger, PhD; Danny Jonigk, MD; Rosa M. Apel, MD; Julia Freise, MD; Hoen-Oh Shin, MD; Desiree Weiberg, MD; Gregor Warnecke, MD; Tobias L. Ross, PhD; Hans-Jürgen Wester, PhD; Benjamin Seeliger, MD; Tobias Welte, MD; Frank M. Bengel, MD; and Antje Prasse, MD

BACKGROUND: Idiopathic pulmonary fibrosis (IPF) is a progressive disease for which two antifibrotic drugs recently were approved. However, an unmet need exists to predict responses to antifibrotic treatment, such as pirfenidone. Recent data suggest that upregulated expression of CXCR4 is indicative of outcomes in IPF.

RESEARCH QUESTION: Can quantitative, molecular imaging of pulmonary CXCR4 expression as a biomarker for disease activity predict response to the targeted treatment pirfenidone and prognosis in patients with IPF?

STUDY DESIGN AND METHODS: CXCR4 expression was analyzed by immunohistochemistry examination of lung tissues and reverse-transcriptase polymerase chain reaction analysis of BAL. PET-CT scanning with the specific CXCR4 ligand ^{68}Ga-pentixafor was performed in 28 IPF patients and compared with baseline clinical characteristics. In 16 patients, a follow-up scan was obtained 6 to 12 weeks after initiation of treatment with pirfenidone. Patients were followed up in our outpatient clinic for ≥ 12 months.

RESULTS: Immunohistochemistry analysis showed high CXCR4 staining of epithelial cells and macrophages in areas with vast fibrotic remodeling. Targeted PET scanning revealed CXCR4 upregulation in fibrotic areas of the lungs, particularly in zones with subpleural honeycombing. Baseline CXCR4 signal demonstrated a significant correlation with Gender Age Physiology stage ($r = 0.44$; $P = .02$) and with high-resolution CT scan score ($r = 0.38$; $P = .04$). Early changes in CXCR4 signal after initiation of pirfenidone treatment correlated with the long-term course of FVC after 12 months ($r = -0.75$; $P = .0008$). Moreover, patients with a high pulmonary CXCR4 signal on follow-up PET scan after 6 weeks into treatment demonstrated a statistically significant worse outcome at 12 months ($P = .002$). In multiple regression analysis, pulmonary CXCR4 signal on follow-up PET scan emerged as the only independent predictor of long-term outcome ($P = .0226$).

INTERPRETATION: CXCR4-targeted PET imaging identified disease activity and predicted outcome of IPF patients treated with pirfenidone. It may serve as a future biomarker for personalized guidance of antifibrotic treatment. CHEST 2021; 159(3):1094-1106

KEY WORDS: biomarker; CXCR4; idiopathic pulmonary fibrosis; imaging; PET

ABBREVIATIONS: DLCO = diffusing lung capacity for carbon monoxide; GAP = Gender Age Physiology; HRCT = high-resolution CT; IPF = idiopathic pulmonary fibrosis; IQR = interquartile range; RT-PCR = reverse-transcriptase polymerase chain reaction; SUV_{max} = maximum standardized uptake value; SUV_{mean} = mean standardized uptake value; TGF-β = transforming growth factor β; VOI = volume-of-interest

AFFILIATIONS: From the Department of Nuclear Medicine (Drs Derlin, Weiberg, Ross, and Bengel), the Institute of Pathology (Dr Jonigk), the Department of Pulmonology (Drs Apel, Freise, Seeliger,

Idiopathic pulmonary fibrosis (IPF) is a fatal disease characterized by progressive respiratory failure, resulting in a median survival of less than 3 years after diagnosis in untreated patients.[1-3] However, interindividual outcome shows great variability. Recently, two antifibrotic drugs, pirfenidone and nintedanib, have been approved for treatment of IPF.[4,5] For both drugs, it has been demonstrated clearly that they attenuate the mean rate of FVC decline over a 12-month period in patients with IPF.[4,5] Some patients show stable or even improved FVC values after 12 months of treatment, whereas others deteriorate rapidly despite antifibrotic treatment.[1,3] Although FVC is a well-accepted primary end point in clinical trials, it needs to be monitored for a 12-month period to draw statistically significantly conclusions. Currently, no markers are available that allow the prediction of long-term response to any of the approved antifibrotic treatments as soon as treatment is started or as treatment progresses.

Recently, the role of CXCR4 and its ligand CXCL12 (also known as SDF-1) in organ fibrosis has been highlighted.[6] The G-protein-coupled receptor CXCR4 has a crucial role in processes relying on cell migration, such as recruitment and homing of cells as well as metastatic spread.[7,8] CXCR4 is expressed in various immune, cancer, stem, and progenitor cells.[8] Several studies have reported CXCR4 expression of monocyte-derived M2 macrophages and have described the role of CXCR4 in homing of bone marrow-derived cells to injured organs.[9-11] CXCR4 signaling mediates epithelial mesenchymal transition of epithelial cells, but also directs cell migration of immune cells and fibrocytes.[8,12] Additional studies have reported reciprocal and amplifying interactions of the transforming growth factor β (TGF-β) and CXCR4 signaling pathways.[6,9,13,14] In various organs, TGF-β is considered to be the master cytokine driving fibrosis and to be related directly to disease activity.[1,3,15,16] Until now, it has been difficult to gauge levels of pulmonary TGF-β production by noninvasive biomarkers. Our own data indicate that *CXCR4* expression of BAL cells is indicative of early mortality in IPF.[17] Hence, we investigated molecular imaging of CXCR4 expression in IPF as a noninvasive biomarker for disease activity and predictive value. For this purpose, we used a highly specific tracer, ^{68}Ga-pentixafor, which recently was introduced for clinical PET imaging of CXCR4 in cardiovascular and oncologic diseases.[18-20]

Methods

Ex Vivo Analysis of CXCR4 *Expression*

Immunohistochemistry analysis for CXCR4 was obtained from the lung tissue of 10 IPF lung explants and three healthy donors, as recently described, using an antibody against CXCR4 (no. ab124824; Abcam).[17,21] Microarray data for *CXCR4* expression of BAL cells were obtained from a recently published dataset consisting of 62 patients with IPF and 20 age-matched healthy volunteers.[17] For the purpose of the current study, we used only the normalized gene expression values for *CXCR4* of the Freiburg cohort.

BAL cells from 16 of the 28 IPF patients who were recruited into the study later were harvested at initial diagnosis during routine diagnostic workup. BAL cells were isolated as recently described,[17,22] harvested in QIAzol lysis reagent (no. 79306; Qiagen), and archived at −80°C. RNA was isolated by RNeasy Mini Kit (no. 74104; Qiagen) in accordance with the standard protocol provided by the manufacturer. Total RNA were reverse transcribed to complementary DNA by using the High-Capacity cDNA Reverse Transcription Kit (no. 4368814; ThermoFisher Scientific). *CXCR4* reverse-transcriptase polymerase chain reaction (RT-PCR) analyses were performed on a TaqMan platform with the following TaqMan primers: *CXCR4* (assay identifier: Hs00976734_m1; no. 4331182; ThermoFisher Scientific) and glyceraldehyde 3-phosphate dehydrogenase (assay identifier: Hs99999905_m1; no. 4331182; ThermoFisher Scientific) as described recently.[23] A cycle threshold value was calculated and used to ascertain the relative level of *CXCR4* messenger RNA by the following formula: relative expression = (2 (cycle threshold of glyceraldehyde 3-phosphate dehydrogenase - cycle threshold of *CXCR4*)) × 10,000 for each complementary DNA sample.

For the analysis of in vitro modulation of *CXCR4* expression, BAL cells from 10 additional patients with IPF were isolated as described recently[22]: 1 × 10^6 BAL cells were cultured in Roswell Park Memorial Institute 1640 medium (no. 11879020; ThermoFisher Scientific) supplemented with 10% fetal bovine serum (no. TMS-013-B; Sigma-Aldrich) and 1% penicillin and streptomycin (no. A2212; Biochrom) for 24 h in an incubator (5% CO_2, 37°C) with or without 2 mM pirfenidone (no. sc-203663; Santa Cruz Biotechnology) or 10 μM SB-431542 (a selective and potent inhibitor of the TGF-β/activin/nodal pathway; no. 72234; STEMCELL technologies) treatment. *CXCR4* expression was tested by RT-PCR as described. In additional experiments, we tested in vitro stimulation of monocyte-derived macrophages and lung tissue slices by TGF-β. Using Ficoll gradient and MACS beads (no. 130-091-153; Miltenyi Biotec), we isolated monocytes from peripheral blood of five additional patients with IPF as indicated by the manufacturer. Monocyte-derived

Welte, and Prasse), the Institute of Radiology (Dr Shin), and the Department of Heart, Thoracic, Transplantation and Vascular Surgery (Dr Warnecke), Hannover Medical School, the Fraunhofer Institute for Toxicology and Experimental Medicine (Drs Jaeger and Prasse), and DZL-BREATH (Drs Apel, Freise, Seeliger, Welte, and Prasse), Hannover, Germany; and the Institute of Radiopharmaceutical Chemistry (Dr Wester), Technical University Munich, Garching, Germany.

FUNDING/SUPPORT: This study was funded by DZL-BREATH and the German research council [Grant KFO311].

CORRESPONDENCE TO: Antje Prasse, MD, Hannover Medical School, Carl-Neuberg-Strasse 1, 30625 Hannover, Germany; e-mail: prasse.antje@mh-hannover.de

DOI: https://doi.org/10.1016/j.chest.2020.08.2043

TABLE 1] Baseline Characteristics of the Study Cohort (N = 28)

Clinical Characteristic	Data
Sex, male/female	22 (79)/6 (21)
Age, y	69 (64-76)
Spirometry at baseline	…
FVC, % predicted	71 (58-89)
TLC, % predicted	71 (59-79)
D_{LCO}, % predicted	48 (37-61)
Resting Pao_2, mm Hg	66 (57-74)
6-min walk distance, m	385 (305-431)
6-min walk test nadir Spo_2, %	85 (81-88)
Extent of fibrosis score (HRCT), No. (%),	…
0	0 (0)
1	4 (14)
2	12 (43)
3	8 (29)
4	4 (14)

Data are presented as No. (%) or median (interquartile range). D_{LCO} = diffusing lung capacity for carbon monoxide; HRCT = high-resolution CT; Spo_2 = oxygen saturation as measured by pulse oximetry; TLC = total lung capacity.

macrophages were generated by stimulating isolated monocytes for five days with granulocyte-macrophage colony-stimulating factor (1 ng/mL; no. 11343123; Immunotools) in Roswell Park Memorial Institute 1640 medium supplemented with 10% human serum, 100,000 U/L penicillin and 100 mg/L streptomycin. Thereafter, cells were stimulated for 48 h with recombinant TGF-β (2 ng/mL; Immunotools) in Roswell Park Memorial Institute 1640 medium supplemented with 100,000 U/L penicillin and 100 mg/L streptomycin; after this, surface CXCR4 expression (CD184 PE; no. 130-098-354; Miltenyi Biotec) was analyzed by flow cytometry using protocols as described.[22,24] Precision-cut lung slices were obtained from three lung explants of patients with fibrotic lung diseases, as recently described, and were cultured in vitro for 28 days in 1:1 bronchial epithelial cell growth medium (BEGM BulletKit medium [no. CC-3170;Lonza] and Gibco DMEM-Dulbecco's Modified Eagle Medium [no. 11965092; ThermoFisher Scientific]) and stimulated with or without TGF-β (2 ng/mL; Immunotools).[25] Medium was replaced every other day. After 28 days, precision-cut lung slices were harvested, formalin fixed, and paraffin embedded. Immunohistochemistry analysis for CXCR4 expression of precision-cut lung slices materials was performed as described above.

Clinical Cohort

Patients: Twenty-eight patients (Table 1) were diagnosed with IPF according to the 2018 diagnostic criteria set forth together by the American Thoracic Society, European Respiratory Society, Japanese Respiratory Society, and Latin American Thoracic Society[2,26,27] and underwent baseline ^{68}Ga-pentixafor PET. All patients were examined during their initial clinical workup, were treatment-naïve, and gave written consent to participate in studies of the German Center for Lung Research (DZL) and, in particular, in studies investigating biomarkers of disease progression and treatment outcomes in IPF. The local institutional review board approved the data analysis. None of the patients were being administered steroid or immunosuppressant therapy at the time of imaging. Pulmonary function tests, 6-min walk test, and capillary blood gas analysis were performed within four weeks before ^{68}Ga-pentixafor PET scanning and during routine clinical follow-up every three months. Noninvasive PET imaging was obtained for clinical purposes, and ^{68}Ga-pentixafor was used according to §13.2b of the German Pharmaceuticals Act. In 16 patients, follow-up imaging was obtained 6 to 12 weeks after initiation of treatment with pirfenidone. The 12 remaining patients were treated with nintedanib. Preliminary imaging and in vitro data in five patients suggested that nintedanib induced CXCR4 upregulation in the context of TGF-β signaling. Because of this observation, we did not perform further PET scans in these patients. For pirfenidone treatment, we applied a dose-escalating regimen and started with a dose of 267 mg 3 times daily for 7 days, then 574 mg 3 times daily for 7 days, and then escalated to the final dose of 801 mg 3 times daily. All of the 16 patients treated with pirfenidone tolerated the dose of 3 × 801 mg daily until the last follow-up visit. Patients were followed up in our outpatient clinic for ≥ 12 months. None of the patients were lost to follow-up or died.

^{68}Ga-Pentixafor Synthesis: Material for synthesis of ^{68}Ga-pentixafor was obtained by Scintomics. Synthesis was performed as described previously[28,29] at Hannover Medical School's Department of Nuclear Medicine (Hannover, Germany) using a ^{68}Ge/^{68}Ga generator (ITG Garching) connected to a Scintomics good radiopharmaceutical practice synthesis module.

Clinical Imaging: All study data were obtained using a dedicated PET/CT system (Biograph mCT Flow; Siemens) equipped with an extended field-of-view lutetium oxyorthosilicate PET component, a 128-slice spiral CT component, and a magnetically driven table optimized for continuous scanning. The patients received an IV injection of 132 MBq (interquartile range [IQR], 91-158 MBq) of ^{68}Ga-pentixafor. Imaging started with a low-dose nonenhanced helical CT (120 kV; mA modulated; pitch, 1.2; reconstructed axial slice thickness, 5.0 mm) performed for attenuation correction of PET acquisitions. PET images of the entire body then were acquired using continuous bed motion at a speed of 2.0 mm/s for head and neck and 0.5 mm/s for chest and abdomen at 60 min after injection. All studies were reconstructed using time-of-flight and point-spread function information combined with an iterative algorithm (Ultra HD; Siemens Healthcare; settings: 2 iterations; 21 subsets; matrix, 200; zoom, 1.0; Gaussian filter, 5.0). Standardized uptake values of normalized by body weight were calculated from Ultra HD PET images. In addition, noncontrast breath-hold high-resolution CT (HRCT) scanning (120 kV, mA modulated) of the chest was performed to obtain contiguous 1.0-mm cross-sectional slices throughout the thorax. Raw data were reconstructed using the reconstruction kernels B31f and B70f and were displayed at window settings suitable for viewing the lung parenchyma.

PET/CT Image Analysis: Transaxial PET, CT, and fused PET/CT images were analyzed in a random order and blinded for further clinical information on a dedicated workstation equipped with a commercial software package (syngo.via VB30A; Siemens Healthcare) by an expert in PET/CT reading (13 years of experience).

PET images were evaluated visually for the presence of elevated radiotracer uptake in lung parenchyma in areas of usual interstitial pneumonia pattern on CT scans. Then, ^{68}Ga-pentixafor uptake was quantified using a 3-D volume-of-interest (VOI) technique with isocontour thresholding at a maximum standardized uptake value (SUV_{max}) threshold of 45%, yielding a mean standardized uptake value (SUV_{mean}) and SUV_{max} of usual interstitial pneumonia areas.

Separate measurements were performed in three subpleural regions in each lung lobe, and values for each region then were averaged for the subsequent statistical analysis. Similar analyses were performed for assessment of tracer uptake in unaffected lung parenchyma without fibrotic changes. Tracer uptake in mediastinal and hilar lymph nodes was assessed in three thoracic lymph node stations using 3-D VOIs with isocontour thresholding and were averaged for the subsequent statistical analysis. In addition, tracer uptake (SUV_{mean}) in the spleen and bone marrow was recorded to evaluate systemic interactions. As a control measurement to address variability between scans, SUV_{mean} of liver (average of three VOIs) and blood pool (average of three VOIs placed inside the superior vena cava) was determined. The end points were not corrected for air volumes or tissue density because we used serial measurements in the same patient and assumed no major changes in air volumes or tissue density in the short observation time. This assumption was supported by stable CT findings.

To assess the reproducibility of the PET analysis, the analysis of pulmonary tracer uptake was repeated by a second reader (4 years of experience). Interrater agreement was good to excellent (intraclass correlation coefficient, 0.95 for analysis of SUV_{max} and 0.88 for analysis of SUV_{mean}), underlining high reproducibility of the image analysis.

Baseline and follow-up HRCT findings were scored using a standardized form, as previously described[30]: the overall extent of fibrosis (ie, extent of reticulation and honeycombing) was determined for each entire lung using a 5-point scale (0, no involvement; 1, 1%-25% involvement; 2, 26%-50% involvement; 3, 51%-75% involvement; and 4, 76%-100% involvement).

Clinical Parameters

Pulmonary function tests were performed routinely with a standard methodology according to the European Respiratory Society and American Thoracic Society recommendations.[31] After treatment, decreasing FVC was defined as any reduction in FVC, whereas all other outcomes were considered to be stable. The Gender Age Physiology (GAP) index, a staging system for patients with IPF, was calculated using gender, age, FVC, and diffusing lung capacity for carbon monoxide (DLCO).[32]

Statistical Analysis

Continuous variables were expressed as median with IQR. Categorical variables were presented with absolute and relative frequencies. For between-group comparisons of continuous data, *P* values were calculated by the Student *t* test or Wilcoxon test, as appropriate. The Pearson correlation coefficient *r* was used to correlate imaging findings. Tracer uptake in lung lobes was compared using a one-way analysis of variance with Tukey's multiple comparisons test. Multiplicity-adjusted *P* values were reported. Ex vivo validation data among study groups were analyzed using the paired Student *t* test. The Fisher exact test was used to test the association between changes in FVC and changes in imaging parameters. Receiver operating characteristic curve analysis was performed to obtain standardized uptake value cutoffs for FVC outcomes. Simple linear regression analysis and multivariate linear regression analysis were performed to identify predictors of long-term outcome in terms of FVC. Survival by *CXCR4* expression was compared by Kaplan-Meier method univariate Cox regression. A *P* value of less than .05 was regarded as statistically significant. Statistical analysis and graph generation were performed using GraphPad Prism version 7 and 8 software (GraphPad Software) and RStudio version 1.2.5033 software (RStudio PBC).

Results

Ex Vivo Analysis of Specimens

In IPF tissue specimens, immunohistochemistry revealed high expression of CXCR4 by macrophages, lymphocytes, and epithelial cells compared with normal tissues (Fig 1A-D). Notably, airway epithelial cells lining honeycomb cysts and epithelial cells covering fibroblast foci showed positive staining results for CXCR4; however, neither the fibroblasts nor endothelial cells showed positive results for CXCR4 expression. In normal lung tissue, a weak CXCR4 expression by macrophages was detectable, and no CXCR4 expression was observed in normal alveolar epithelial cells.

In IPF BAL cells, *CXCR4* gene expression data were obtained from a previously published dataset obtained by microarrays.[17] Normalized *CXCR4* expression values were increased significantly in BAL cells from IPF patients compared with healthy control subjects (12.7×10^3 [12.3-13.7] vs 12.2×10^3 [10.0-12.8]; $P = .011$) (Fig 1E). High *CXCR4* gene expression of BAL cells (more than the median of 12.7×10^3) in IPF patients was associated with early mortality with univariate Cox regression (unadjusted hazard ratio, 2.0; 95% CI, 1.1-3.7; $P = .025$) (Fig 1F).

Pharmacologic Modulation of CXCR4 Expression

Modulation of *CXCR4* expression of BAL cells derived from 10 treatment-naïve patients with IPF was tested in vitro. Treatment with pirfenidone for 24 h did not change *CXCR4* expression significantly. By contrast, *CXCR4* expression as measured by RT-PCR was downregulated significantly by treatment with SB-431542, an anaplastic lymphoma kinase inhibitor that interferes in TGF-β signaling (Fig 1G). Moreover, *CXCR4* expression of monocyte-derived macrophages from IPF patients increased with statistical significance after TGF-β stimulation ($P = .042$) (Fig 1H). Repetitive TGF-β stimulation of IPF tissue slices over 4 weeks increased *CXCR4* expression in epithelial cells (Fig 1I, 1J).

Upregulated In Vivo CXCR4 Signal

^{68}Ga-pentixafor PET showed variable degrees of CXCR4 upregulation in fibrotic areas, predominantly in areas of subpleural honeycombing (Figs 2, 3). The median maximum HRCT score was 2 (IQR, 2-3). The mean CXCR4 signal in fibrotic areas was 2.2 (IQR, 1.9-2.5), and the maximum CXCR4 signal was 3.9 (IQR, 3.4-4.1).

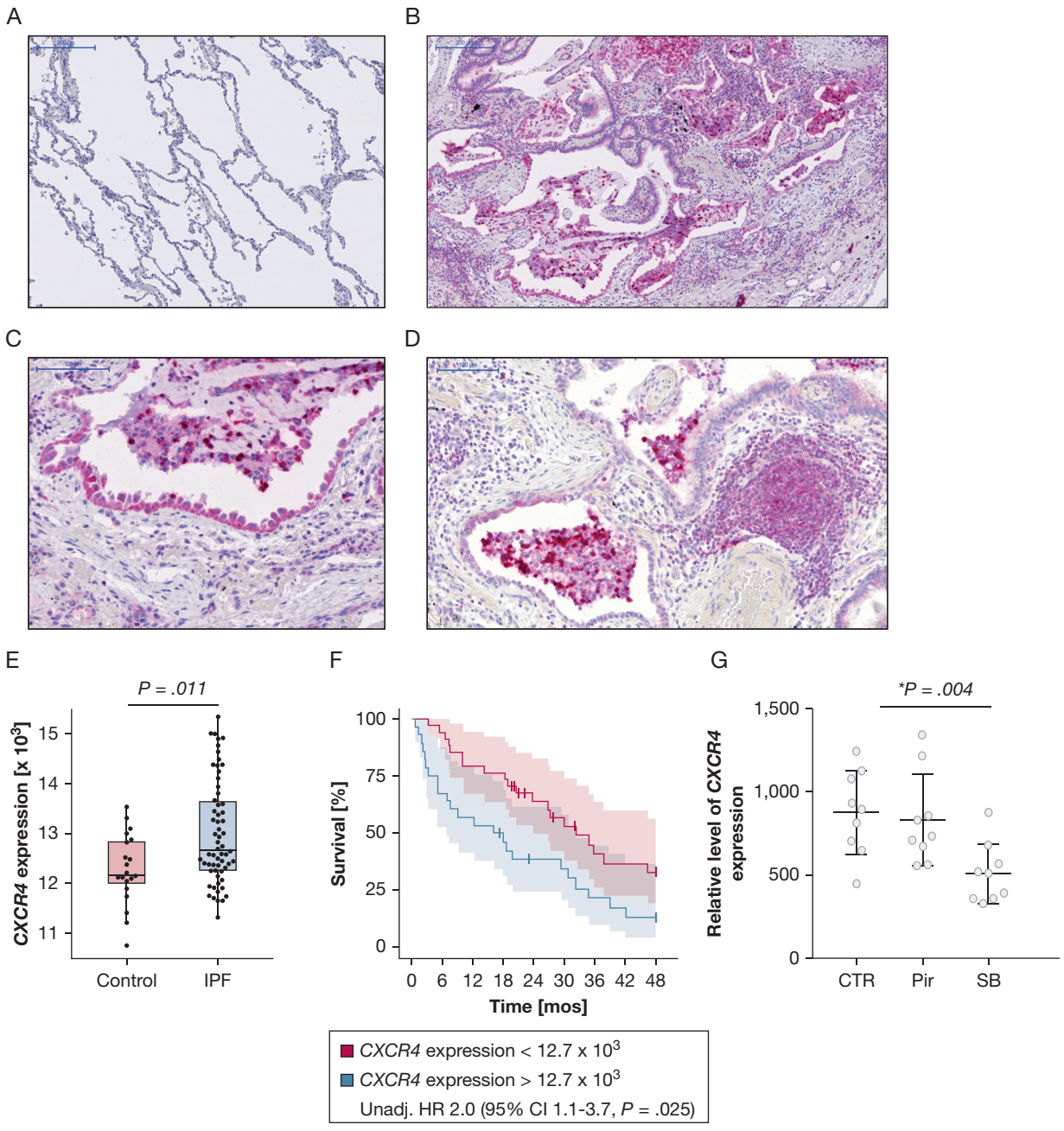

Figure 1 – *A-J, High* CXCR4 *expression in fibrotic areas of idiopathic pulmonary fibrosis (IPF) lungs and especially by macrophages, lymphocytes, and epithelial cells.* CXCR4 *expression was evaluated by immunohistochemistry in healthy (A) and IPF (B-D) lungs.* CXCR4 *expression was significantly upregulated in IPF lungs and particularly in the areas of vast fibrotic remodeling.* CXCR4 *expression was high in macrophages, lymphocytes, and epithelial cells, but absent in fibroblasts.* CXCR4 *expression was high in epithelial cells covering fibroblast foci and honeycomb cysts, but absent in alveolar epithelial cells lining normal alveoli. Scale bars, A,B: 200 µm, C,D: 100 µm. E, Normalized* CXCR4 *expression by microarray in BAL cells from IPF patients vs healthy control participants. F, 48-month survival of IPF patients stratified by median CXCR4 expression with associated 95% CIs (shaded areas). Patients were censored at end of follow-up. The unadjusted hazard ratio (HR) with 95% CI was calculated by univariate Cox regression model. G, BAL cells from IPF patients were stimulated in vitro with Pir or SB, which inhibits transforming growth factor β (TGF-β) signaling. H, Representative original registration of the CXCR4 fluorescence intensity (histogram) by flow cytometry. CXCR4 expression was upregulated significantly by TGF-β stimulated (blue) compared with unstimulated (red) monocyte-derived macrophages. Compared with unstimulated control (I), TGF-β stimulation (J) also upregulated CXCR4 expression by epithelial cells in cultured precision cut lung slices of lung tissues from IPF patients. CTR = healthy control participants; Pir = pirfenidone; SB = SB-431542.*

The CXCR4 signal demonstrated a significant correlation with maximum HRCT score of lungs (SUV_{max}: $r = 0.38$; $P = .04$; SUV_{mean}: $r = 0.43$; $P = .02$). When the regional CXCR4 expression pattern was analyzed on PET, CXCR4 upregulation was highest in the lower lobes. Maximum CXCR4 signal (SUV_{max}) in

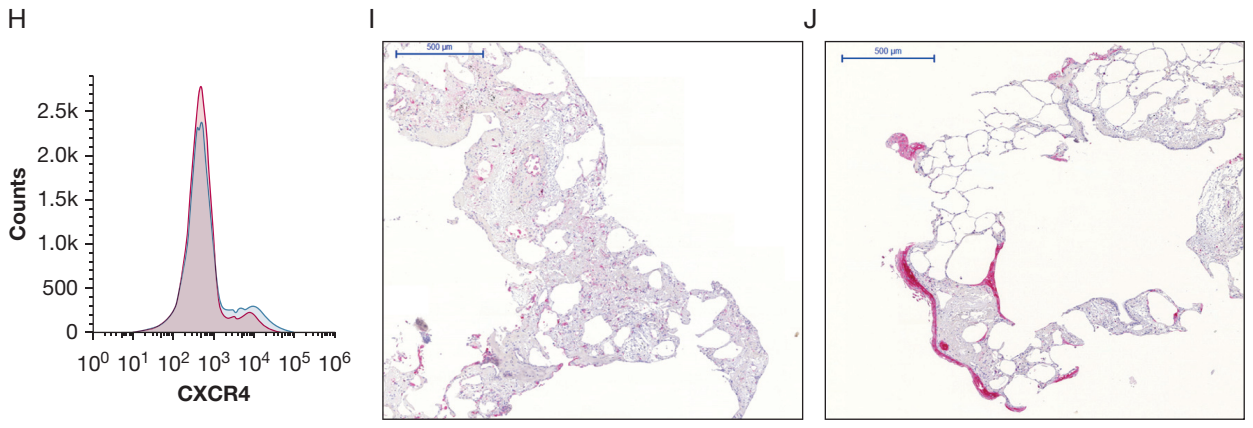

Figure 1 – *Continued*

the lower lobes was significantly higher than in upper lobes (4.4 vs 3.6; $P = .005$) or in the middle lobe (2.9; $P < .0001$). Mean CXCR4 signal (SUV_{mean}) in the lower lobes also was significantly higher than in the upper lobes (2.6 vs 2.1; $P = .001$) or in the middle lobe (1.8; $P < .0001$).

Increased CXCR4 signal in fibrotic areas was paralleled by elevated CXCR4 signal in thoracic lymph nodes in all 28 patients (100%). CXCR4 signal in fibrotic areas demonstrated a significant correlation with CXCR4 signal in spleen (SUV_{mean}, 6.0; IQR, 5.0-6.4; $r = 0.38$; $P = .04$) and lymph nodes (SUV_{mean}, 3.6; IQR, 3.3-4.5; $r = 0.44$; $P = .02$), highlighting systemic interactions (Fig 2). The correlation between CXCR4 signal in fibrotic areas and bone marrow did not reach statistical significance (SUV_{mean}, 2.8; IQR, 2.2-3.2; $r = 0.35$; $P = .07$).

Correlates of PET CXCR4 Signal

Bronchoscopy with BAL of the middle lobe was performed in a subcohort of the patients. RNA of BAL cells for further evaluation of CXCR4 expression by RT-PCR was available from 16 of the 28 IPF patients. We observed a statistically significant correlation between the log CXCR4 expression of BAL cells and the CXCR4 PET signal (SUV_{max}) of the middle lobe ($r = 0.57$; $P = .02$) (Fig 2C).

Regarding associations with clinical parameters, the maximum CXCR4 signal (SUV_{max}) demonstrated a significant correlation with GAP stage and predicted mortality ($r = 0.44$; $P = .02$). A significant inverse correlation was found between CXCR4 signal and 6-min walk test nadir oxygen saturation as measured by pulse oximetry ($r = -0.48$; $P = .04$). No significant correlation was found between CXCR4 signal and 6-min walk distance ($r = -0.35$; $P = .13$), resting Pa_{O_2} ($r = -0.38$; $P = .11$), FVC ($r = -0.13$; $P = .50$), total lung capacity ($r = 0.05$; $P = .80$), D_{LCO} ($r = -0.14$, $P = .50$), and leukocyte count in peripheral blood ($r = 0.09$; $P = .64$).

The maximum HRCT score also demonstrated a significant correlation with both GAP stage and predicted mortality ($r = 0.48$; $P = .009$) and GAP index ($r = 0.51$; $P = .006$). Both FVC ($r = -0.55$; $P = .002$) and D_{LCO} ($r = -0.52$; $P = .006$), but not total lung capacity ($r = -0.31$; $P = .12$), were associated significantly with the maximum HRCT score. No significant correlation was found between HRCT score and resting Pa_{O_2} ($r = 0.14$; $P = .56$), 6-min walk distance ($r = -0.33$; $P = .15$), or 6-min walk test nadir oxygen saturation as measured by pulse oximetry ($r = -0.12$; $P = .62$).

PET CXCR4 Signal and Outcomes

After commencing treatment with pirfenidone, follow-up PET scanning (Fig 3) was carried out at a median of 55 days (IQR, 46-95 days) after the initial PET scan. At the follow-up PET scan, CXCR4 downregulation (SUV_{mean}) by 13% (IQR, 9%-16%) was observed in fibrotic areas in 11 patients (69%), paralleled by stable FVC at the follow-up PET scan. Five patients (31%) showed an increase in CXCR4 signal by a median of 10% (IQR, 5%-10%) in fibrotic areas, accompanied by a decrease in predicted FVC by a median of −5% (IQR, −4% to −8%) in three of the five patients at the follow-up PET scan. CXCR4 signal in thoracic lymph nodes ($P = .50$), spleen ($P = .82$), and bone marrow ($P = .84$) was unchanged after treatment with pirfenidone. Likewise, PET signal in unaffected lung parenchyma ($P = .40$), liver ($P = .67$), and blood pool ($P = .50$) was

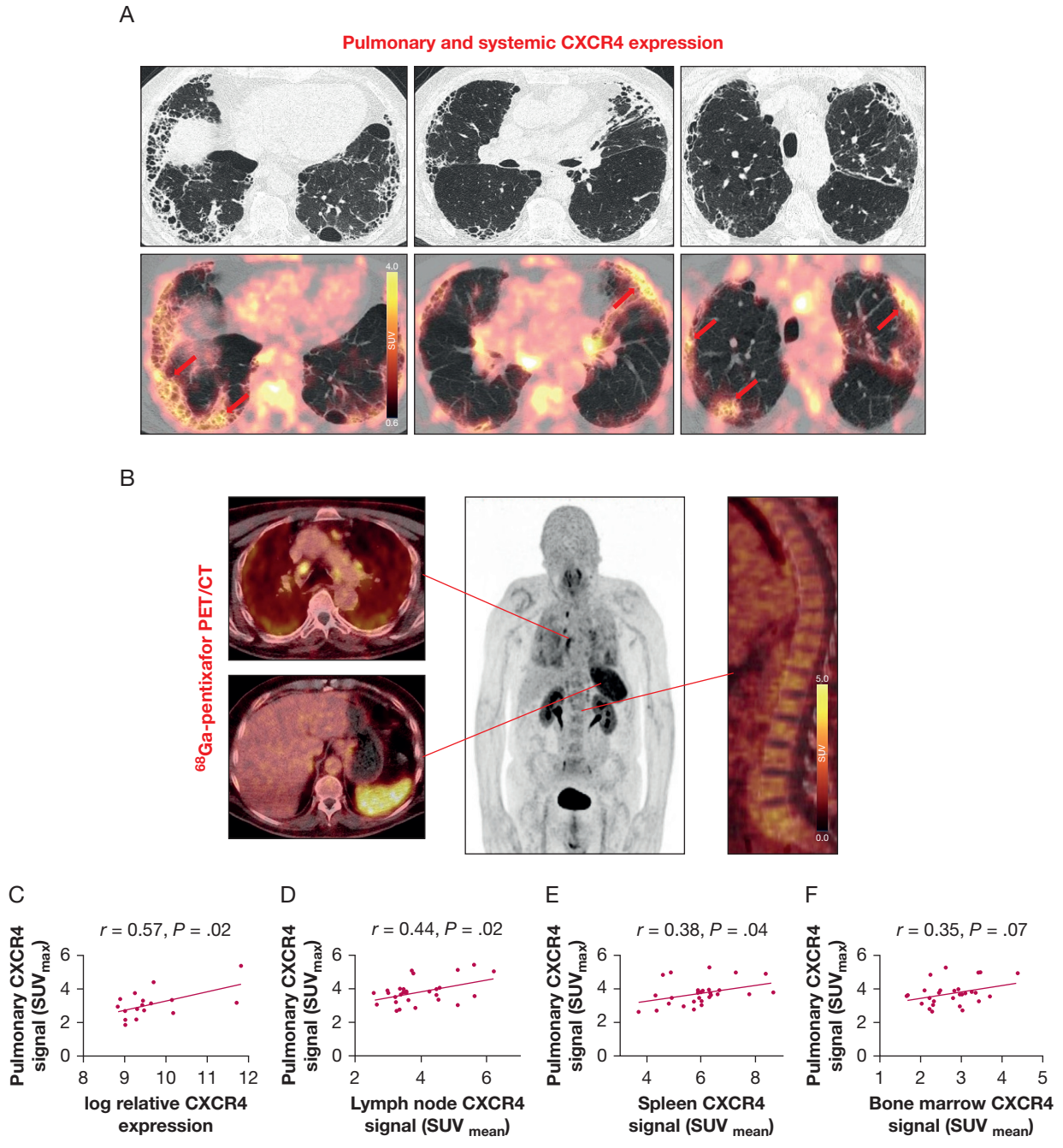

Figure 2 – *A-F, Targeted PET/CT scanning detects pulmonary and systemic CXCR4 expression in IPF patients. A, Elevated CXCR4 signal (arrows) in fibrotic areas with subpleural honeycombing in an IPF patient as determined by ^{68}Ga-pentixafor PET scan. B, Systemic CXCR4 expression quantified in thoracic lymph nodes, spleen, and bone marrow. C, CXCR4 signal of the middle lobe correlates with log relative CXCR4 expression of BAL cells as measured by reverse-transcriptase polymerase chain reaction (P = .02). D-F, Increased CXCR4 expression in fibrotic areas of lungs paralleled by elevated CXCR4 expression in lymph nodes (D) (P = .02), spleen (E) (P = .04), and bone marrow (F) (P = .07), highlighting systemic interactions. SUV_{max} = maximum standardized uptake value; SUV_{mean} = mean standardized uptake value. See Figure 1 legend for expansion of other abbreviations.*

unchanged after treatment, showing that the significant changes in fibrotic areas indeed have been caused by pharmacologic modulation. Short-term deteriorating FVC was associated significantly with an increase in CXCR4 signal in fibrotic areas on the follow-up PET scan ($P = .02$). By contrast, the maximum HRCT score was unchanged on follow-up HRCT. Deteriorating FVC therefore was not associated with alterations of parenchymal changes on follow-up HRCT ($P = 1.0$).

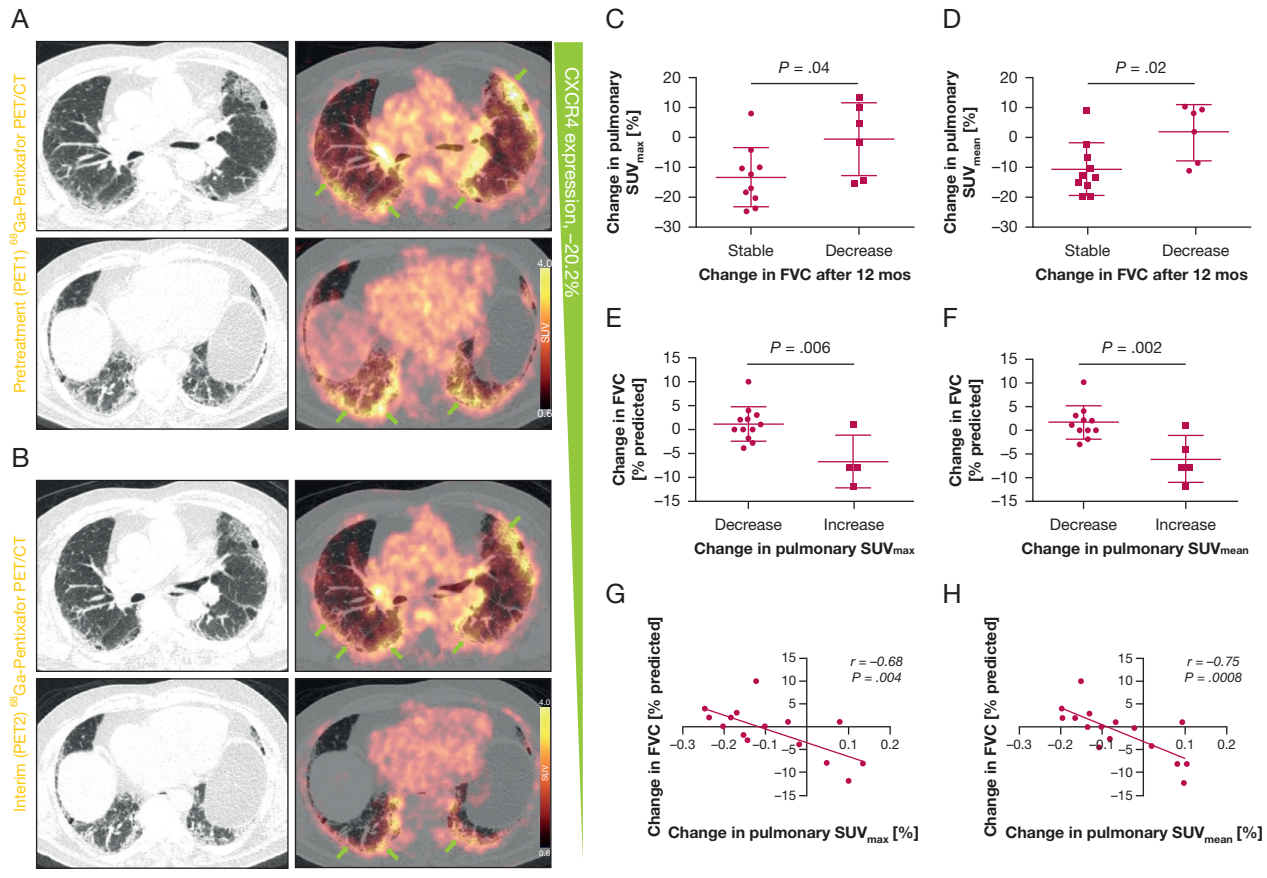

Figure 3 – *A-H, Targeted PET/CT scan detects early changes in pulmonary CXCR4 expression in IPF patients after commencing treatment with pirfenidone. Early change in pulmonary CXCR4 expression was quantified using CXCR4-targeted ^{68}Ga-pentixafor PET scanning. A, B, Exemplary images of a patient with decreasing pulmonary CXCR4 signal after commencing pirfenidone treatment and stable FVC at 12 months: before treatment at baseline (A) and after 6 weeks of pirfenidone treatment (B). C-H, After initiation of pirfenidone therapy, the decrease in CXCR4 signal between the initial and the follow-up PET scan is less in patients with worse outcome (C, D). Patients with worse outcome demonstrate an increase in CXCR4 expression at the follow-up PET scan (E, F). Early change in CXCR4 signal between the initials and the follow-up PET scan is statistically significantly correlated with outcome, as determined by FVC decline after 12 months of pirfenidone treatment (G, H). See Figure 1 and 2 legends for expansion of other abbreviations.*

Regarding long-term outcome, the change in CXCR4 signal between the initial PET scan and the follow-up PET scan was significantly different between patients with a decrease in FVC and those with stable FVC (SUV_{max}, +2% [IQR,−15% to +11%] vs −15% [IQR, −9% to −21%]; $P = .04$; SUV_{mean}, +5% [IQR, −10% to +10%] vs. -13% [IQR, −5% to −17%]; $P = .02$). Accordingly, short-term change in CXCR4 signal between the initial PET scan and the follow-up PET scan demonstrated a significant correlation with long-term change in FVC (SUV_{max}: $r = −0.68$; $P = .004$; SUV_{mean}: $r = −0.75$; $P = .0008$) (Fig 3). In addition, patients treated with pirfenidone who demonstrated a long-term decrease in FVC showed significantly higher pulmonary CXCR4 expression (SUV_{max}, 3.8 [IQR, 3.5-4.5] vs 3.1 [IQR, 2.9-3.6]; $P = .008$; SUV_{mean}, 2.3 [IQR, 2.3-2.5] vs 2.0 [IQR, 1.7-2.1]; $P = .002$) at the follow-up PET scan than patients with stable FVC. Accordingly, CXCR4 signal at the follow-up PET scan demonstrated a significant correlation with long-term change in FVC (SUV_{max}: $r = −0.58$; $P = .02$; SUV_{mean}: $r = −0.66$; $P = .005$) (Fig 4). Baseline CXCR4 signal at the initial PET scan was not predictive of outcome. CXCR4 signal at the initial PET scan and the follow-up PET scan in lymph nodes ($P = .48$ and $P = .20$, respectively), spleen ($P = .31$ and $P = .71$, respectively), and bone marrow ($P = .89$ and $P = .85$, respectively) was not different between patients with deteriorating FVC and those with stable FVC.

Linear regression analysis revealed that early changes in FVC at the follow-up PET scan ($P = .0036$), pulmonary CXCR4 signal at the follow-up PET scan (SUV_{max}, $P = .0194$; SUV_{mean}, $P = .0051$), and short-term change in pulmonary CXCR4 signal between the initial PET scan and the follow-up PET scan (SUV_{max}, $P = .0040$; SUV_{mean}, $P = .0008$) predicted long-term outcome at

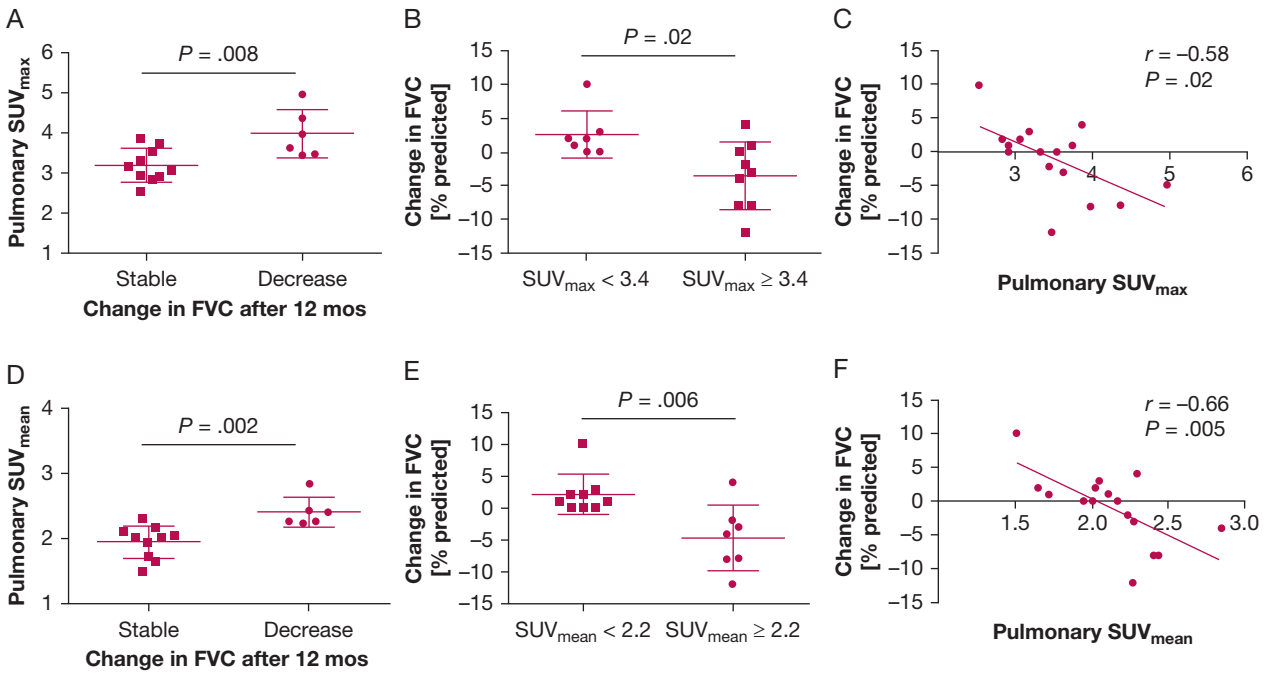

Figure 4 – *A-F, CXCR4 expression at targeted the follow-up PET scan early after commencing treatment with pirfenidone is associated with outcome. A, Pulmonary CXCR4 expression as measured by SUV_{max} at the follow-up PET scan is higher in patients with worse outcome. B, Patients with an $SUV_{max} \geq 3.4$ at the follow-up PET scan achieved a significantly worse outcome than patients with a lower SUV_{max}. C, SUV_{max} values at the follow-up PET scan correlated significantly with decline in FVC after 12 months of pirfenidone treatment. D, Pulmonary CXCR4 expression as measured by SUV_{mean} at the follow-up PET scan is higher in patients with worse outcome. E, Patients with an $SUV_{mean} \geq 2.2$ at the follow-up PET scan achieved a significantly worse outcome than patients with a lower SUV_{mean}. F, SUV_{mean} values at the follow-up PET scan correlated significantly with decline in FVC after 12 months of pirfenidone treatment. See Figure 2 legend for expansion of abbreviations.*

12 months. In multiple regression analysis, pulmonary CXCR4 signal at the follow-up PET scan emerged as the only independent predictor of long-term outcome (SUV_{mean}, $P = .0226$) (Table 2).

Discussion

Recently, we demonstrated that high gene expression of CXCR4 is upregulated in IPF and associated with early mortality.[17] Ex vivo studies gave evidence that CXCR4 is highly expressed in macrophages, lymphocytes, and epithelial cells in IPF specimens and is upregulated by TGF-β stimulation. Therefore, we used clinical molecular imaging for the in vivo assessment of systemic and local thoracic CXCR4 expression in IPF. CXCR4 expression was highest in the areas of highest fibrotic burden (eg, at the subpleural and dorsobasal regions), including areas of honeycombing, which was confirmed by CXCR4 immunohistochemistry analysis. In a cohort of 16 patients treated with pirfenidone, we demonstrated that both high residual CXCR4 expression on the follow-up PET scan and early changes in CXCR4 signal predicted outcomes after 12 months.

Immunohistochemistry for CXCR4 expression revealed abundant CXCR4 expression in IPF tissues compared with normal lung. Microarray data confirmed this result. CXCR4 protein expression was high in macrophages, lymphocytes, and airway epithelial cells accumulating in the lung parenchyma. Airway epithelial cells lining honeycomb cysts and fibroblast foci expressed CXCR4. It is of interest that our immunohistochemistry data clearly demonstrate that macrophages also express very high levels of CXCR4 in IPF tissues. Previous studies have demonstrated that CXCR4 is expressed by monocyte-derived macrophages homing to injured organs and that an increase in subtypes of monocyte-derived macrophages is detected easily by ^{68}Ga-pentixafor PET scan.[9,19,33,34] ^{68}Ga-pentixafor PET scanning has recently emerged as a highly specific means for noninvasive imaging and quantification of in vivo CXCR4 expression. It exhibits high CXCR4 affinity, high in vivo stability, and high and specific target accumulation, and blockade with the CXCR4 antagonist AMD3100 abolishes the signal in vivo.[19,28] Using ex vivo autoradiography and immunohistochemistry, other studies have demonstrated that ^{68}Ga-pentixafor PET identifies $CXCR4^{+}$ cells in preclinical and clinical settings.[19,20,35] Against this background, it seems reasonable that ^{68}Ga-pentixafor PET detects CXCR4-

TABLE 2] Predictors of Long-Term Outcome After Initiation of Pirfenidone Treatment

Parameter	Univariate Linear Regression Analysis				Multiple Regression Analysis			
	Slope	SE	95% CI	*P* Value	Estimate	SE	95% CI	*P* Value
FVC, % predicted	…	…	…	…	…	…	…	…
At initial PET scan	−0.07401	0.09644	−0.2809 to 0.1328	.4556	…	…	…	…
At follow-up PET scan	0.02646	0.1001	−0.1883 to 0.2412	.7954	…	…	…	…
Change at the follow-up PET scan	0.6360	0.1819	0.2459 to 1.026	**.0036**	0.2441	0.1308	−0.04749 to 0.5356	.0917
SUV_{max} at initial PET scan	−0.6042	2.198	−5.318 to 4.110	.7874	…	…	…	…
SUV_{mean} at initial PET scan	−1.699	4.096	−10.48 to 7.085	.6845	…	…	…	…
SUV_{max} the follow-up PET scan	−4.968	1.881	−9.002 to 0.9328	**.0194**	6.723	3.659	−1.430 to 14.88	.0960
SUV_{mean} the follow-up PET scan	−10.74	3.236	−17.68 to −3.803	**.0051**	−18.44	6.853	−33.71 to −3.174	**.0226**
Change in pulmonary SUV_{max}, %	−29.54	8.582	−47.95 to −11.13	**.0040**	−15.22	17.93	−55.17 to 24.73	.4158
Change in pulmonary SUV_{mean}, %	−36.53	8.647	−55.07 to −17.98	**.0008**	−9.935	19.36	−53.07 to 33.20	.6190

P values in bold denote statistical significance.
SUV_{max} = maximum standardized uptake value; SUV_{mean} = mean standardized uptake value.

positive macrophages and airway epithelial cells accumulating in IPF lungs, both recently shown to be linked with disease outcome.[36-38] Indeed, looking even closer, we found that CXCR4 expression is linked to TGF-β signaling effects.[9,13,14] TGF-β is considered to be the master cytokine of fibrosis and particularly of IPF.[1,3,15] Stimulation of either macrophages or lung tissues by TGF-β led to an increase in CXCR4 expression in both monocyte-derived macrophages and epithelial cells, confirming previous findings.[11,14,39] Moreover, *CXCR4* expression of alveolar macrophages, which are considered already to be full-blown stimulated by TGF-β in situ,[40] was downregulated in the presence of the anaplastic lymphoma kinase inhibitor SB-431542, which blocks TGF-β type I receptor signaling. Pirfenidone, which does not directly interfere in TGF-β signaling, had no effect on *CXCR4* expression after 24 h of in vitro treatment. Of interest, in vitro treatment of BAL cells with pirfenidone did not change *CXCR4* expression. In summary, our in vitro data corroborated the hypothesis that *CXCR4* expression is linked to key pathomechanisms orchestrating IPF and is not directly affected by pirfenidone treatment.[41]

When analyzing the pulmonary CXCR4 expression on ^{68}Ga-pentixafor PET/CT scan, all patients showed CXCR4 upregulation in fibrotic areas, predominantly in the subpleural and dorsobasal regions of the lungs and particularly in areas of honeycombing and dense fibrosis. The CXCR4 signal of the middle lobe obtained by ^{68}Ga-pentixafor PET/CT scan correlated with the BAL cell CXCR4 expression as measured by RT-PCR. The data are in line with our immunohistochemistry data that showed CXCR4 expression by honeycomb cysts and cells accumulating in the surrounding interstitium. CXCR4 signal in terms of both SUV_{max} and SUV_{mean} was significantly higher in lower lobes in this study. Thus, CXCR4 signal was highest in the areas of the lung that were most affected by IPF. It is of interest that the CXCR4 signal also was elevated in thoracic lymph nodes and the spleen, correlating significantly with the pulmonary fibrotic areas, which highlights systemic interaction.

The CXCR4 signal demonstrated a significant correlation with GAP stage and predicted mortality, meaning that patients with high CXCR4 expression had an unfavorable prognosis and increased predicted mortality based on clinical parameters. However, baseline CXCR4 signal did not correlate with baseline FVC percent and DLCO percent predicted values, both

accepted markers of disease extent. These findings indicate that CXCR4 signal intensity is not correlated directly with disease extent, but rather, correlates with disease activity and may provide prognostic information. Other studies have looked at different PET tracers for characterization of other aspects of IPF. Umeda and colleagues[42] demonstrated that dual-time-point ^{18}F-fluorodeoxyglucose PET scanning is strongly predictive of earlier deterioration of pulmonary function and higher mortality in patients with IPF. However, fluorodeoxyglucose is a substrate of glucose metabolism and represents a rather unspecific marker of different aspects of disease. Other groups have aimed to visualize more specific targets in IPF, such as macrophages using cathepsin protease probes for PET.[43] However, imaging of CXCR4 expression as a marker of disease activity in IPF has not been evaluated before.

In this study, we obtained follow-up CXCR4 imaging in 16 patients after initiation of treatment with pirfenidone. Interestingly, CXCR4 downregulation by 13% (IQR, 9%−16%) was observed in fibrotic areas in 69% of patients, paralleled by stable lung function parameters. The other 31% of patients showed an increase in CXCR4 signal by a median of 10% (IQR, 5%−10%) in fibrotic areas. An increase in CXCR4 expression at the follow-up PET scan was associated significantly with a rapid decline in FVC after a 12-month observation period. Conversely, patients with a decrease in CXCR4 expression at the follow-up PET scan achieved a more favorable outcome. Moreover, a pulmonary CXCR4 signal at the follow-up PET scan emerged as the only independent predictor of long-term outcome ($P = .0226$) in multiple regression analysis. However, the absence of significance of FVC ($P = .0917$) in this analysis may be related to the limited sample size. It is conceivable that both parameters may emerge as significant predictors in a larger independent prospective trial. Although PFT values may reach statistical significance in a larger cohort, from a clinical perspective, subtle intraindividual changes in FVC are hard to interpret based on the variance of the PFT method. Against the background of the above-mentioned findings, our data suggest that CXCR4 PET imaging was able to characterize disease activity in IPF patients. Our finding that the early changes in CXCR4 signal intensity correlate with long-term outcome after 12 months may indicate that the signal was altered by the pharmacologic intervention. Because of the single-arm study design, we cannot determine whether pirfenidone had a direct effect on CXCR4 signal intensity. However, our in vitro data suggest that there is no direct effect of pirfenidone on CXCR4 expression. Thus, our data clearly suggest that short-term changes in CXCR4 signal intensity detect changes in disease activity, which are related to long-term outcome. Further prospective studies are needed to evaluate whether CXCR4 imaging can be used for the monitoring of treatment effects. Of note, the normal variability in PET uptake measurements between different scans in the absence of a therapeutic intervention has been shown to be negligible. In a study evaluating the CXCR4 signal in atherosclerotic plaque, the uptake in various arterial wall lesions remained unchanged between a baseline PET scan and a follow-up scan after 111 ± 38 days without specific antiatherosclerotic therapy (signal intensity, 1.8 ± 0.3 vs 1.8 ± 0.3; $P = .93$), supporting that variability in PET uptake measurements in organs can be neglected.[44] In line with these findings, PET signal in reference measurements (eg, unaffected lung parenchyma) was unchanged between scans. Recently, pirfenidone, has been approved for the treatment of IPF. Although its precise mechanism of action currently is not understood fully, pirfenidone has shown antifibrotic and antiinflammatory properties in in vitro systems and animal models of fibrosis, partly because of the inhibition of TGF-β signaling.[45] Several randomized controlled trials have shown a clinically meaningful effect of pirfenidone on markers of disease progression, such as decline in FVC and progression-free survival.[4,46] Given that pirfenidone treatment is associated with considerable treatment costs and that not all patients will respond to pirfenidone, early confirmation of molecular response by means of CXCR4-targeted PET/CT scan could help to identify patients who will benefit most from that therapy. However, larger prospective studies are needed, not only to confirm the potential of CXCR4-targeted PET/CT scan for therapy monitoring, but also to support further that the observed posttherapeutic alterations in CXCR4 expression are associated consistently with clinical outcomes. In accordance with other publications, our data additionally highlight a potential functional role of CXCR4 in IPF, which needs to be addressed in further studies.[47,48]

This study had limitations. First, the relatively small size of the study population limited the statistical power. However, the observed associations are robust and significant. Second, direct histopathologic validation

could not be obtained for both practical and ethical reasons, but we found that BAL CXCR4 gene expression correlated with the CXCR4 PET signal. The role of CXCR4 in IPF is well established, and the high specificity of the radiotracer used has been demonstrated in other settings,[19,28] thus supporting our approach. The promoter region of the *CXCR4* gene contains responsive elements for hypoxia, cyclic adenosine monophosphate, and proto-oncogene tyrosine-protein kinase Src.[49,50] CXCR4 imaging therefore may reflect not only TGF-β signaling, but also other relevant pathways of IPF not addressed by our in vitro studies. Third, the imaging protocol was based on previously published experience with ^{68}Ga-pentixafor in different clinical settings such as cardiovascular diseases. Optimization of the protocol in terms of respiratory gating or longer tracer uptake times may improve imaging data further.

Conclusions

Targeted PET imaging with ^{68}Ga-pentixafor identifies the local and general CXCR4 expression pattern in lung parenchyma and systemic organs. In IPF, CXCR4 imaging may have a role in monitoring disease activity and treatment response and in predicting outcomes in patients treated with pirfenidone.

Acknowledgments

Author contributions: T. D., F. B., and A. P. provided study design and concept. T. D., B. J., H. S., R. M. A., J. F., D. J., D. W., G. W., T. L. R., and A. P. acquired the data. T. D., B. J., H. S., R. M. A., J. F., D. J., D. W., G. W., T. L. R., B. S., and A. P. analyzed and interpreted the data. T .D., B. J., and A. P. drafted the manuscript. T. D., B. J., H. S., R. M. A., J. F., D. J., D. W., G. W., T. L. R., H. W., B. S., T. W., F. M. B., and A. P. critically revised the manuscript for important intellectual content. T. D., B. J., B. S., and A. P. conducted statistical analysis. T. D., B. J., G. W., H. S., T. R., H.-J. W., F. M. B., and A. P. provided administrative, technical, or material support. T. D. and A. P. supervised the study.

Financial/nonfinancial disclosures: The authors have reported to *CHEST* the following: H. J. W. is coinventor of Pentixafor, consultant and advisory board member for Scintomics, and holds ownership interest including patents. Scintomics has joined 1717 LSV to create PentixaPharm GmbH. J. F. and R. M. A. received lecture fees from Boehringer Ingelheim. D. J. received lecture fees from Boehringer Ingelheim and Roche. A. P. submitted a patent on pulmonary *CXCR4* upregulation by nintedanib. A. P. is a consultant to Boehringer Ingelheim, Roche, Pliant, Indalo Therapeutics, Nitto Denko, and Astra Zeneca and received lecture fees from Boehringer Ingelheim, Roche, Novartis, Chiesi, and Astra Zeneca. None declared (T. D., B. J., F. M. B., H. S., D. W., G. W., B. S., T. W., T. R.).

Role of sponsors: The sponsors (DZL BREATH and German research council had no role in the design of the study, the collection and analysis of the data, or the preparation of the manuscript.

Other contributions: The authors thank Dr S. Rittinghausen for technical support and Bobbie Smith for careful text editing.

References

1. King TE Jr, Pardo A, Selman M. Idiopathic pulmonary fibrosis. *Lancet*. 2011;378(9807):1949-1961.
2. Raghu G, Collard HR, Egan JJ, et al. An official ATS/ERS/JRS/ALAT statement: idiopathic pulmonary fibrosis: evidence-based guidelines for diagnosis and management. *Am J Respir Crit Care Med*. 2011;183(6):788-824.
3. Lederer DJ, Martinez FJ. Idiopathic pulmonary fibrosis. *N Engl J Med*. 2018;379(8):797-798.
4. King TE Jr, Bradford WZ, Castro-Bernardini S, et al. A phase 3 trial of pirfenidone in patients with idiopathic pulmonary fibrosis. *N Engl J Med*. 2014;370(22):2083-2092.
5. Richeldi L, du Bois RM, Raghu G, et al. Efficacy and safety of nintedanib in idiopathic pulmonary fibrosis. *N Engl J Med*. 2014;370(22):2071-2082.
6. Yuan A, Lee Y, Choi U, Moeckel G, Karihaloo A. Chemokine receptor Cxcr4 contributes to kidney fibrosis via multiple effectors. *Am J Physiol Renal Physiol*. 2015;308(5):F459-F472.
7. Zlotnik A, Burkhardt AM, Homey B. Homeostatic chemokine receptors and organ-specific metastasis. *Nat Rev Immunol*. 2011;11(9):597-606.
8. Burger JA, Kipps TJ. CXCR4: a key receptor in the crosstalk between tumor cells and their microenvironment. *Blood*. 2006;107(5):1761-1767.
9. Bertran E, Caja L, Navarro E, et al. Role of CXCR4/SDF-1 alpha in the migratory phenotype of hepatoma cells that have undergone epithelial-mesenchymal transition in response to the transforming growth factor-beta. *Cell Signal*. 2009;21(11):1595-1606.
10. Hughes R, Qian BZ, Rowan C, et al. Perivascular M2 macrophages stimulate tumor relapse after chemotherapy. *Cancer Res*. 2015;75(17):3479-3491.
11. Chatterjee M, von Ungern-Sternberg SN, Seizer P, et al. Platelet-derived CXCL12 regulates monocyte function, survival, differentiation into macrophages and foam cells through differential involvement of CXCR4-CXCR7. *Cell Death Dis*. 2015;6:e1989.
12. Dupin I, Allard B, Ozier A, et al. Blood fibrocytes are recruited during acute exacerbations of chronic obstructive pulmonary disease through a CXCR4-dependent pathway. *J Allergy Clin Immunol*. 2016;137(4):1036-1042 e1037.
13. Feng YF, Yuan F, Guo H, Wu WZ. TGF-beta1 enhances SDF-1-induced migration and tube formation of choroid-retinal endothelial cells by up-regulating CXCR4 and CXCR7 expression. *Mol Cell Biochem*. 2014;397(1-2):131-138.
14. Bertran E, Crosas-Molist E, Sancho P, et al. Overactivation of the TGF-beta pathway confers a mesenchymal-like phenotype and CXCR4-dependent migratory properties to liver tumor cells. *Hepatology*. 2013;58(6):2032-2044.
15. Khalil N, Parekh TV, O'Connor R, et al. Regulation of the effects of TGF-beta 1 by activation of latent TGF-beta 1 and differential expression of TGF-beta receptors (T beta R-I and T beta R-II) in idiopathic pulmonary fibrosis. *Thorax*. 2001;56(12):907-915.
16. Selman M, King TE, Pardo A. Idiopathic pulmonary fibrosis: prevailing and evolving hypotheses about its pathogenesis and implications for therapy. *Ann Intern Med*. 2001;134(2):136-151.
17. Prasse A, Binder H, Schupp JC, et al. BAL cell gene expression is indicative of outcome and airway basal cell involvement in idiopathic pulmonary fibrosis. *Am J Respir Crit Care Med*. 2019;199(5):622-630.
18. Philipp-Abbrederis K, Herrmann K, Knop S, et al. In vivo molecular imaging of chemokine receptor CXCR4 expression in patients with advanced multiple myeloma. *EMBO Mol Med*. 2015;7(4):477-487.
19. Thackeray JT, Derlin T, Haghikia A, et al. Molecular imaging of the chemokine receptor CXCR4 after acute myocardial infarction. *JACC Cardiovasc Imaging*. 2015;8(12):1417-1426.

20. Derlin T, Sedding DG, Dutzmann J, et al. Imaging of chemokine receptor CXCR4 expression in culprit and nonculprit coronary atherosclerotic plaque using motion-corrected [(68)Ga]pentixafor PET/CT. *Eur J Nucl Med Mol Imaging*. 2018;45(11):1934-1944.
21. Demmer O, Dijkgraaf I, Schumacher U, et al. Design, synthesis, and functionalization of dimeric peptides targeting chemokine receptor CXCR4. *J Med Chem*. 2011;54(21):7648-7662.
22. Prasse A, Pechkovsky DV, Toews GB, et al. A vicious circle of alveolar macrophages and fibroblasts perpetuates pulmonary fibrosis via CCL18. *Am J Respir Crit Care Med*. 2006;173(7):781-792.
23. Huppertz C, Jager B, Wieczorek G, et al. The NLRP3 inflammasome pathway is activated in sarcoidosis and involved in granuloma formation. *Eur Respir J*. 2020;55(3):1900119.
24. Pechkovsky DV, Prasse A, Kollert F, et al. Alternatively activated alveolar macrophages in pulmonary fibrosis-mediator production and intracellular signal transduction. *Clin Immunol*. 2010;137(1):89-101.
25. Hess A, Wang-Lauenstein L, Braun A, et al. Prevalidation of the ex-vivo model PCLS for prediction of respiratory toxicity. *Toxicol In Vitro*. 2016;32:347-361.
26. Raghu G, Remy-Jardin M, Myers JL, et al. Diagnosis of idiopathic pulmonary fibrosis. An official ATS/ERS/JRS/ALAT clinical practice guideline. *Am J Respir Crit Care Med*. 2018;198(5):e44-e68.
27. American Thoracic Society. Idiopathic pulmonary fibrosis: diagnosis and treatment. International consensus statement. American Thoracic Society (ATS) and the European Respiratory Society (ERS). *Am J Respir Crit Care Med*. 2000;161(2 Pt 1):646-664.
28. Gourni E, Demmer O, Schottelius M, et al. PET of CXCR4 expression by a (68)Ga-labeled highly specific targeted contrast agent. *J Nucl Med*. 2011;52(11):1803-1810.
29. Martin R, Juttler S, Muller M, Wester HJ. Cationic eluate pretreatment for automated synthesis of [(6)(8)Ga]CPCR4. 2. *Nucl Med Biol*. 2014;41(1):84-89.
30. Lynch DA, Godwin JD, Safrin S, et al. High-resolution computed tomography in idiopathic pulmonary fibrosis: diagnosis and prognosis. *Am J Respir Crit Care Med*. 2005;172(4):488-493.
31. Graham BL, Brusasco V, Burgos F, et al. Executive summary: 2017 ERS/ATS standards for single-breath carbon monoxide uptake in the lung. *Eur Respir J*. 2017;49(1):16E0016.
32. Ley B, Ryerson CJ, Vittinghoff E, et al. A multidimensional index and staging system for idiopathic pulmonary fibrosis. *Ann Intern Med*. 2012;156(10):684-691.
33. Reiter T, Kircher M, Schirbel A, et al. Imaging of C-X-C motif chemokine receptor CXCR4 expression after myocardial infarction with [(68)Ga]pentixafor-PET/CT in correlation with cardiac MRI. *JACC Cardiovasc Imaging*. 2018;11(10):1541-1543.
34. Weiberg D, Thackeray JT, Daum G, et al. Clinical molecular imaging of chemokine receptor CXCR4 expression in atherosclerotic plaque using (68)Ga-pentixafor PET: correlation with cardiovascular risk factors and calcified plaque burden. *J Nucl Med*. 2018;59(2):266-272.
35. Derlin T, Gueler F, Brasen JH, et al. Integrating MRI and chemokine receptor CXCR4-targeted PET for detection of leukocyte infiltration in complicated urinary tract infections after kidney transplantation. *J Nucl Med*. 2017;58(11):1831-1837.
36. Fernandez IE, Greiffo FR, Frankenberger M, et al. Peripheral blood myeloid-derived suppressor cells reflect disease status in idiopathic pulmonary fibrosis. *Eur Respir J*. 2016;48(4):1171-1183.
37. Moore BB, Fry C, Zhou Y, et al. Inflammatory leukocyte phenotypes correlate with disease progression in idiopathic pulmonary fibrosis. *Front Med*. 2014;1(56):56.
38. Liu YZ, Saito S, Morris GF, Miller CA III, Li J, Lefante JJ. Proportions of resting memory T cells and monocytes in blood have prognostic significance in idiopathic pulmonary fibrosis. *Genomics*. 2018;111(6):1343-1350.
39. Chen S, Tuttle DL, Oshier JT, et al. Transforming growth factor-beta1 increases CXCR4 expression, stromal-derived factor-1alpha-stimulated signalling and human immunodeficiency virus-1 entry in human monocyte-derived macrophages. *Immunology*. 2005;114(4):565-574.
40. Morris DG, Huang X, Kaminski N, et al. Loss of integrin alpha(v)beta6-mediated TGF-beta activation causes Mmp12-dependent emphysema. *Nature*. 2003;422(6928):169-173.
41. Selman M, Martinez FJ, Pardo A. Why does an aging smoker's lung develop idiopathic pulmonary fibrosis and not chronic obstructive pulmonary disease? *Am J Respir Crit Care Med*. 2019;199(3):279-285.
42. Umeda Y, Demura Y, Morikawa M, et al. Prognostic value of dual-time-point 18F-FDG PET for idiopathic pulmonary fibrosis. *J Nucl Med*. 2015;56(12):1869-1875.
43. Withana NP, Ma X, McGuire HM, et al. Non-invasive imaging of idiopathic pulmonary fibrosis using cathepsin protease probes. *Sci Rep*. 2016;6:19755.
44. Li X, Heber D, Leike T, et al. [68Ga]Pentixafor-PET/MRI for the detection of chemokine receptor 4 expression in atherosclerotic plaques. *Eur J Nucl Med Mol Imaging*. 2018;45(4):558-566.
45. Sun YW, Zhang YY, Ke XJ, Wu XJ, Chen ZF, Chi P. Pirfenidone prevents radiation-induced intestinal fibrosis in rats by inhibiting fibroblast proliferation and differentiation and suppressing the TGF-beta1/Smad/CTGF signaling pathway. *Eur J Pharmacol*. 2018;822:199-206.
46. Noble PW, Albera C, Bradford WZ, et al. Pirfenidone in patients with idiopathic pulmonary fibrosis (CAPACITY): two randomised trials. *Lancet*. 2011;377(9779):1760-1769.
47. Antoniou KM, Soufla G, Lymbouridou R, et al. Expression analysis of angiogenic growth factors and biological axis CXCL12/CXCR4 axis in idiopathic pulmonary fibrosis. *Connect Tissue Res*. 2010;51(1):71-80.
48. Griffiths K, Habiel DM, Jaffar J, et al. Anti-fibrotic effects of CXCR4-targeting i-body AD-114 in preclinical models of pulmonary fibrosis. *Sci Rep*. 2018;8(1):3212.
49. Bao Y, Wang Z, Liu B, et al. A feed-forward loop between nuclear translocation of CXCR4 and HIF-1alpha promotes renal cell carcinoma metastasis. *Oncogene*. 2019;38(6):881-895.
50. Cristillo AD, Highbarger HC, Dewar RL, Dimitrov DS, Golding H, Bierer BE. Up-regulation of HIV coreceptor CXCR4 expression in human T lymphocytes is mediated in part by a cAMP-responsive element. *FASEB J*. 2002;16(3):354-364.